Hydrodynamic stress on small colloidal aggregates in shear flow using Stokesian dynamics

Ryohei Seto,[1,*] Robert Botet,[2] and Heiko Briesen[1,†]

[1]*Chair for Process Systems Engineering, Technische Universität München, Weihenstephaner Steig 23, D-85350 Freising, Germany*

[2]*Laboratoire de Physique des Solides, Université Paris-Sud, UMR8502, Bât 510, F-91405 Orsay, France*

(Received 28 June 2011; revised manuscript received 22 September 2011; published 31 October 2011)

The hydrodynamic properties of rigid fractal aggregates have been investigated by considering their motion in shear flow in the Stokesian dynamics approach. Due to the high fluid viscosity and small particle inertia of colloidal systems, the total force and torque applied to the aggregate reach equilibrium values in a short time. Obtaining equilibrating motions for a number of independent samples, one can extract the average hydrodynamic characteristics of the given fractal aggregates. Despite the geometry of these objects being essentially disordered, the average drag-force distributions for aggregates show symmetric patterns. Moreover, these distributions collapse on a single master curve, characteristic of the nature of the aggregates, provided the positions of the particles are rescaled with the geometric radius of gyration. This result can be used to explain the reason why the stress acting on an aggregate and moments of the forces acting on contact points between particles follow power-law behaviors with the aggregate size. Moreover, the values of the exponents can be explained. As a consequence, considering cohesive force typical for colloidal particles, we find that even aggregates smaller than a few dozen particles must experience restructuring when typical shear flow is applied.

DOI: 10.1103/PhysRevE.84.041405 PACS number(s): 82.70.−y, 83.60.Fg, 47.15.G−, 61.43.Hv

I. INTRODUCTION

Systems of colloidal aggregates involve various phenomena from the molecular scale to the nano- or microscale. The interaction between colloidal particles depends on a number of factors: the shape of the particles, their elasticity, the nature of the particle surface, the temperature and chemical properties of the fluid, and so forth. Additionally, complicated hydrodynamic interactions act on them: a particle moving in a fluid will change the velocity field of the fluid, which will result in a change in the motion of the other particles. Due to these factors, the modeling of colloidal system is an important issue and many questions are still pending, even if extensive research efforts in the field have been carried out over many years.

Any approach investigating colloidal aggregates dispersed in a fluid requires knowledge of the adhesion between particles. Nowadays, direct observations are available using novel experimental techniques, such as atomic force microscopy [1–3], optical tweezers [4,5], and confocal microscopy [6]. These direct approaches give valuable insights about the adhesive forces or the mechanical properties of aggregates. However, the particles available for such direct observations are restricted to certain sizes, so the parameter determination for contact models is still incomplete. A variety of approaches have been used as alternative ways of investigating colloidal-aggregate systems. Colloidal aggregates exhibit naturally fractal structures, so their characteristic geometric morphology can be studied using scattering methods, such as small-angle light, x-ray, or neutron scattering [7–9]. However, the hydrodynamic characteristics may depend on a nontrivial way on the geometry. These characteristics are, for example, the sedimentation velocity [10,11], the diffusion constant [12,13], and, more generally, the rheology [14], with all being measured in specific experiments. The hydrodynamic stress experienced by the aggregates is then the key property to investigate and understand, in order to be able to analyze the experimental data properly.

Here, we report a study on the interaction between hydrodynamics and rigid fractal aggregates in shear flow. Situations where colloidal aggregates are exposed to several types of flow are common to various industrial processes in which the control of sizes and morphology for given flow conditions is a central issue. Many observations have been reported recently related to breakup and restructuring of colloidal aggregates by flows [15–24]. In these experiments, hydrodynamic interactions act constantly on the particles within an aggregate and the structure of the stressed aggregate depends directly on the local adhesive forces. To understand the final state of the aggregate, one needs then to simulate both the drag-force and stress distributions.

The first approach to this problem was to model the aggregate as a porous sphere, where the Brinkman's equation is used to evaluate the fluid passing through a porous media [25–28]. This theory requires consideration of a spherical structure with continuous porosity, which could be valid for sufficiently large and compact aggregates. Smaller and/or open-structured aggregates require more detailed simulations. In order to evaluate hydrodynamic interactions acting on individual particles, one needs in principle to deal with the Navier-Stokes equation, considering the proper boundary conditions at the surfaces of the particles. For typical colloidal systems, the particle Reynolds number is significantly small, so the Stokes equation can be used instead. An enormous number of studies of Stokes flow have been carried out in the fields of fluid mechanics and applied mathematics [29]. Though the finite-element method is the most rigorous numerical approach to solve the Stokes equation, the huge calculation cost drastically restricts the size of the aggregates [30]. Alternatively, a formulation using multipole expansions can reduce the calculation cost substantially. Stokesian dynamics (SD) is one of the most successful methods and can be

*setoryohei@me.com

†heiko.briesen@mytum.de

used within a wide range of volume fractions. Actually, just after the development of SD, Bossis *et al.* [31] studied the hydrodynamic stress acting on colloidal aggregates. They found a significant difference between rigid aggregates and aggregation of force-free particles, with different power-law relations between the stress S and the number of particles, N: $S \propto N^{3/d_f}$ for rigid aggregates and $S \propto N$ for aggregation of force-free particles, where d_f is the fractal dimension of the aggregates. SD was also applied to rigid aggregates by Binder *et al.* [32], in which partially sintered agglomerates were investigated with respect to the total drag forces. In their work, they also compared SD to lattice Boltzmann simulations, finding a good agreement except in the region of the sintered necks. Harshe *et al.* [33] explicitly gave the resistance matrix for a rigid fractal aggregate by using SD and discussed the hydrodynamic behavior with an equivalent sphere model, i.e., the hydrodynamic radius, and moreover an equivalent ellipsoid model. Another numerical method that is more accurate for contacting particles was proposed by Filippov [34]. Thus, the hydrodynamic behavior of fractal aggregates has been studied by many groups. However, to the best of our knowledge, there is no work that evaluates the hydrodynamic forces acting on rigid aggregates by explicitly considering their realistic motions in shear flow. There are several simulations of the time evolution for primary particles with effective hydrodynamic interactions [35] or SD [36]. However, the contact models used allow facile restructuring of the aggregates. Consequently, they cannot describe the hydrodynamic properties of aggregates with definite structures.

We report here a strategy to tackle the problem. The target of the present work is to study small-sized open-structured fractal aggregates. For such systems, the assumption of a porous media should not apply. Though we do not deal with the time-evolution phenomena, such as the restructuring and breakup, the realistic motion of a rigid aggregate under shear flow can explicitly be considered. The idea is the same as the problem of finding the terminal velocity of a particle under a constant force in a viscous fluid. Due to the high fluid viscosity and small particle inertia of colloidal systems, the total force and torque acting on an aggregate are expected to reach their equilibrium values quickly. In order to calculate the drag forces and torques, we have used SD. The contents of the paper are as follows: Brief descriptions of fractal aggregates and SD are given in Secs. II A and II B, respectively. In Sec. II C, the torque-balanced motion is introduced. The procedure to determine forces and moments acting on contact points is shown in Sec. II D. The torque-balanced motions are reported in Secs. III A and III B, and the hydrodynamic radii estimated with uniform flow and shear flow are examined in Sec. III C. After that, we report the spatial distribution of the drag forces in Sec. III D. At the end, the forces acting on the contact points are evaluated in Sec. III E. Section IV gives a summary and the conclusion.

II. METHOD

A. Fractal aggregates

The key question of this work is to determine how hydrodynamic interactions change depending on the size and morphology of a colloidal aggregate. In order to prepare several sizes and morphologies, we have used computer algorithms that are commonly used to generates fractal aggregates [37,38]. Such fractal structures are seen in real colloidal systems [39]. As will be explained below, fractal structures follow a simple scaling law. Such scaling laws should cause some systematic size dependence for the hydrodynamic responses, which are the target of this work.

For all of the cases in this paper, the aggregates are composed of primary particles that are rigid spheres of radius a, and the distance between the two particles in contact is always $2a$. The following three models are employed here. The first model is reaction-limited hierarchical cluster-cluster aggregation (CCA) [40]. A CCA cluster consisting of N particles is formed by two CCA clusters of $N/2$ particles, each of which is formed by two CCA clusters of $N/4$ particles, and so on. At each step, the direction to adjoin is chosen randomly. The second model is diffusion-limited particle-cluster aggregation (denoted by DLA) [41], in which a particle moving by random walk collides with a stationary cluster and is fixed to the cluster at that point. It is more probable for the particle to attach to the surface of the cluster, so that "bushy" structures are formed by such a process. Thus, these two models involve randomness in the generated structures. For comparison, as the third model we also examine three-dimensional Vicsek (3D-Vicsek) fractals, which have regular structures (see Fig. 1).

The aggregates generated by these models are known to follow a power-law relation between the radius of gyration, R_g, and the number of primary particles, N:

$$R_g/a = CN^{1/d_f}. \tag{1}$$

The radius of gyration, R_g, is defined as the root-mean-square distance of the particles from the aggregate's center of mass:

$$R_g^2 \equiv \frac{1}{N}\sum_i (\boldsymbol{r}^{(i)} - \boldsymbol{r}_0)^2, \tag{2}$$

where $\boldsymbol{r}^{(i)}$ and $\boldsymbol{r}_0$ are the position of particle i and the center of mass of the aggregate, respectively. The power-law relation (1) is well defined for large particle number ($N \to \infty$), where

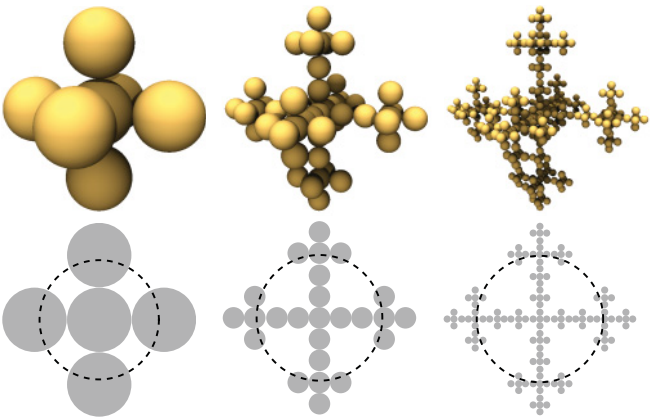

FIG. 1. (Color online) 3D-Vicsek fractals ($N = 7,29,343$) (top row) and their two-dimensional projections (bottom row). The radius of gyration is denoted by the broken circles.

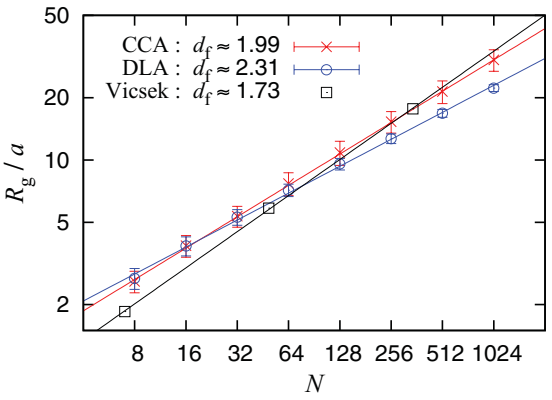

FIG. 2. (Color online) The N dependence of the radius of gyration R_g for CCA, DLA, and 3D-Vicsek fractals. The average values and the standard deviations are plotted.

the value d_f is considered as a fractal dimension. However, we investigate only small aggregates in this work. Even then, such a fractal law is seen for some cases [42]. As Fig. 2 shows, the average values of CCA clusters follow the power law very well and the ones by the DLA model do reasonably. The lines indicate the results of fitting by using the least-squares method with the assumption of a power-law behavior in Eq. (1) for 256 samples of CCA and DLA clusters, each of size $N = 2^{k+2}$ ($k = 1, \ldots, 8$). We obtained $(d_f, C) = (1.99 \pm 0.01, 0.93 \pm 0.01)$ for CCA and $(d_f, C) = (2.31 \pm 0.01, 1.14 \pm 0.01)$ for DLA. These error estimations are based on a confidence interval of 95% for the linear regression of the data sets $(\log N, \log R_g)$. It is worth noting that such small sizes of DLA clusters show a crossover behavior, i.e., the fractal dimension corresponding to the local slope between adjacent data points changes from a smaller value to the asymptotic value 2.5 with increasing size. For the 3D-Vicsek fractal model, though the theoretical value of the fractal dimension is $d_f = \log 7 / \log 3$ (≈ 1.77), the N-R_g relations for the small sizes ($N = 7, 49, 343$) lead to $(d_f, C) \approx (1.73, 0.60)$. The radii of gyration for 3D-Vicsek fractals are shown by their two-dimensional projections (see the bottom row of Fig. 1).

B. Stokesian dynamics

We employ Stokesian dynamics as devised by Durlofsky *et al.* [43] and Brady and Bossis [44]. Stokesian dynamics is a numerical method to deal with the Stokes equation, which is the zero-Reynolds-number limit of the Navier-Stokes equation. This method does not provide the solution of Stokes equation, i.e., the velocity and pressure fields of the fluid; instead, the relations between the hydrodynamic interactions acting on the particles and their relative velocities from an imposed flow are determined. The evaluation starts from the solution of the Stokes equation for a point force, which is written by using the Oseen tensor. As a result of the linearity of the Stokes equation, the fluid-velocity disturbance caused by particles can be formulated as a superposition of point forces, which is given in an integral form. Since particles are assumed to be spheres, multipole expansions can be applied for the integrals. After arranging these expanded terms, the linear relations between the force moments and the velocity moments are obtained [45]. For standard SD, the expansion is truncated at first order. This truncation causes serious errors when the particles move within a close distance of each other. In order to avoid such errors, the two-body exact solution is used to correct interactions between two approaching particles, which is called the lubrication correction. As the result, SD is considered as an effective method to deal with a wide range of volume fractions.

In order to evaluate hydrodynamic interactions in shear flow, the force-torque-stresslet (FTS) version of SD is required. The imposed flow is expressed with constant vectors and tensors, i.e., the translational velocity $\boldsymbol{U}^\infty$, vorticity $\boldsymbol{\Omega}^\infty$, and rate of strain E^∞:

$$\boldsymbol{U}^\infty(\boldsymbol{r}) = \boldsymbol{U}^\infty + \boldsymbol{\Omega}^\infty \times \boldsymbol{r} + \mathsf{E}^\infty \cdot \boldsymbol{r}. \tag{3}$$

The shear flow, $\boldsymbol{U}^\infty(\boldsymbol{r}) = Gz\boldsymbol{e}_x$, is given by the following nonzero elements: $(\Omega^\infty)_y = (E^\infty)_{xz} = (E^\infty)_{zx} = G/2$, where G and $\boldsymbol{e}_x$ indicate the shear rate and the unit vector along the x axis, respectively. The hydrodynamic interactions acting on a particle, the drag forces $\boldsymbol{F}^{(i)}$, torques $\boldsymbol{T}^{(i)}$, and stresslets $\mathsf{S}^{(i)}$, are given as a linear combination of the relative velocities from the imposed flow, the translational velocities $\boldsymbol{U}^{(j)} - \boldsymbol{U}^\infty(\boldsymbol{r}^{(j)})$, and rotational velocities $\boldsymbol{\Omega}^{(j)} - \boldsymbol{\Omega}^\infty$ of all particles $j = 1, \ldots, N$, and the rate of strain $-\mathsf{E}^\infty$. This linear combination is given by using the so-called grand resistance matrix R [43]:

$$\begin{pmatrix} \boldsymbol{F} \\ \boldsymbol{T} \\ \boldsymbol{S} \end{pmatrix} = -\mathsf{R} \cdot \begin{pmatrix} \boldsymbol{U} - \boldsymbol{U}^\infty \\ \boldsymbol{\Omega} - \boldsymbol{\Omega}^\infty \\ -\boldsymbol{E}^\infty \end{pmatrix}, \quad \mathsf{R} \equiv \begin{pmatrix} \mathsf{R}_{\mathrm{FU}} & \mathsf{R}_{\mathrm{FO}} & \mathsf{R}_{\mathrm{FE}} \\ \mathsf{R}_{\mathrm{TU}} & \mathsf{R}_{\mathrm{TO}} & \mathsf{R}_{\mathrm{TE}} \\ \mathsf{R}_{\mathrm{SU}} & \mathsf{R}_{\mathrm{SO}} & \mathsf{R}_{\mathrm{SE}} \end{pmatrix}. \tag{4}$$

These vectors contain elements for all particles, e.g., $\boldsymbol{F} \equiv (F_x^{(1)}, F_y^{(1)}, F_z^{(1)}, \ldots, F_x^{(N)}, F_y^{(N)}, F_z^{(N)})$. Since both the stresslet and rate-of-strain tensors are symmetric and traceless, the five independent elements are denoted as vector forms, such as $\boldsymbol{S}^{(i)} \equiv (S_{xx}^{(i)}, S_{xy}^{(i)}, S_{xz}^{(i)}, S_{yz}^{(i)}, S_{yy}^{(i)})$. Therefore, the size of the grand resistance matrix R is $11N \times 11N$. In this work, we have used the numerical library developed by Ichiki [46] for obtaining it.

In this paper, we consider the situation where a colloidal aggregate of finite size is exposed to an imposed flow. There, the flow is disturbed systematically by particles being close to each other. A systematic error depending on the size of the aggregate is expected because the lubrication correction, namely, the two-body solution, does not take such disturbance of the imposed flow into account. This kind of systematic error is undesirable. However, we consider only rigid aggregates in this work. In this case, the relative velocities between any two particles within an aggregate are always zero. We may omit the lubrication correction because it is effective only for the finite relative velocity between particles nearly touching. Bossis *et al.* [31] and Harshe *et al.* [33] have also taken the same approach to study aggregate systems. We have also checked that this approach yields similar results for the rigid fractal aggregates reported by Filippov [34] (see Sec. III C).

For comparison, the free-draining approximation (FDA) has also been employed, in which the Stokes formula is used for each individual particle. By following the same manner as Eq. (4), the resistance matrix of the FDA has nonzero elements only for the self-parts, i.e., $\mathsf{R}_{\mathrm{FU}}^{(\mathrm{FDA})} = 6\pi\mu a \mathsf{I}_{3N}$,

$\mathsf{R}_{\mathrm{TO}}^{(\mathrm{FDA})} = 8\pi\mu a^3 \mathsf{I}_{3N}$, and $\mathsf{R}_{\mathrm{SE}}^{(\mathrm{FDA})} = (20/3)\pi\mu a^3 \mathsf{I}_{5N}$, where μ is the viscosity of the fluid and I_n is the $n \times n$ identity matrix. Though the FDA is valid only for the dilute limit, it is used for the simulation of the time evolution because of its simplicity and low calculation cost [30,47–49].

C. The torque-balanced motion in shear flow

Here, the dilute limit of a colloidal-aggregate system is studied, with aggregates consisting of a certain number of primary particles existing far from others. They are freely suspended in the fluid phase, so that they are carried by the shear flow. Our interest is in examining the drag forces acting on individual particles for such a situation. In this work, we investigate hydrodynamic behavior of rigid fractal aggregates, so that neither their elastic deformation nor restructuring are considered. Furthermore, in order to avoid carrying out a time-evolution simulation, we took an approximate strategy as follows. Due to the small inertia of colloidal particles in comparison to the hydrodynamic interactions, their motions satisfy balancing conditions about the drag forces and torques after a short relaxation time. So, the balancing condition with a given configuration of particles is solved in this work. For a rigid object of arbitrary shape, a linear relation between the force and the velocity holds as a consequence of the linearity of the Stokes equation. The relation is given by a single 11×11 matrix for the FTS level. Since a rigid aggregate consisting of spheres is considered here, the matrix elements can be explicitly derived from the grand resistance matrix R [Eq. (4)]. The outline of the derivation will be shown in the following paragraph, but more explicit equations can be found in Harshe *et al*. [33].

Due to the rigidity of the aggregate, the translational and angular velocities of a particle i relate to the translational and angular velocities of the aggregate $(\boldsymbol{U}_{\mathrm{ag}}, \boldsymbol{\Omega}_{\mathrm{ag}})$. So, the relative velocities from a imposed flow can be written as

$$\begin{aligned} \boldsymbol{U}^{(i)} - \boldsymbol{U}^{\infty}(\boldsymbol{r}^{(i)}) &= \boldsymbol{U}_{\mathrm{ag}} - \boldsymbol{U}^{\infty}(\boldsymbol{r}_0) + (\boldsymbol{\Omega}_{\mathrm{ag}} - \boldsymbol{\Omega}^{\infty}) \\ &\quad \times \boldsymbol{l}^{(i)} - \mathsf{E}^{\infty} \cdot \boldsymbol{l}^{(i)}, \\ \boldsymbol{\Omega}^{(i)} - \boldsymbol{\Omega}^{\infty} &= \boldsymbol{\Omega}_{\mathrm{ag}} - \boldsymbol{\Omega}^{\infty}, \end{aligned} \tag{5}$$

where $\boldsymbol{l}^{(i)} \equiv \boldsymbol{r}^{(i)} - \boldsymbol{r}_0$. By substituting Eq. (5) in Eq. (4), the force, torque, and stresslet acting on an individual particle i are also given in terms of the velocities of the aggregate and the positions $\boldsymbol{l}^{(j)}$ of all the particles $j = 1, \ldots, N$. The total force, torque, and stresslet acting on the rigid aggregate $(\boldsymbol{F}_{\mathrm{ag}}, \boldsymbol{T}_{\mathrm{ag}}, \mathsf{S}_{\mathrm{ag}})$ are composed of the contributions for the individual particles:

$$\begin{aligned} \boldsymbol{F}_{\mathrm{ag}} &= \sum_i \boldsymbol{F}^{(i)}, \quad \boldsymbol{T}_{\mathrm{ag}} = \sum_i \{\boldsymbol{T}^{(i)} + \boldsymbol{l}^{(i)} \times \boldsymbol{F}^{(i)}\}, \\ \mathsf{S}_{\mathrm{ag}} &= \sum_i \left\{ \mathsf{S}^{(i)} + \frac{1}{2}(\boldsymbol{l}^{(i)} \otimes \boldsymbol{F}^{(i)} + \{\boldsymbol{l}^{(i)} \otimes \boldsymbol{F}^{(i)}\}^{\mathrm{T}}) \right. \\ &\quad \left. - \frac{1}{3}(\boldsymbol{l}^{(i)} \cdot \boldsymbol{F}^{(i)})\mathsf{I} \right\}, \end{aligned} \tag{6}$$

where the symbol $\otimes$ indicates the dyadic product. It is worth noting that the larger the size of an aggregate, the more significant are the contributions of the drag forces $\boldsymbol{F}^{(i)}$ to the total torque $\boldsymbol{T}_{\mathrm{ag}}$ and stresslet S_{ag}. After rearranging Eqs. (6), one can obtain a linear expression between the total forces and the velocities for the rigid aggregate:

$$\begin{pmatrix} \boldsymbol{F}_{\mathrm{ag}} \\ \boldsymbol{T}_{\mathrm{ag}} \\ \boldsymbol{S}_{\mathrm{ag}} \end{pmatrix} = -\mathsf{R}_{\mathrm{ag}} \cdot \begin{pmatrix} \boldsymbol{U}_{\mathrm{ag}} - \boldsymbol{U}^{\infty}(\boldsymbol{r}_0) \\ \boldsymbol{\Omega}_{\mathrm{ag}} - \boldsymbol{\Omega}^{\infty} \\ -\boldsymbol{E}^{\infty} \end{pmatrix}. \tag{7}$$

Thus, all elements of the 11×11 resistance matrix R_{ag} are uniquely determined by the geometrical configuration of the aggregate. Arbitrary motion of the aggregate $(\boldsymbol{U}_{\mathrm{ag}}, \boldsymbol{\Omega}_{\mathrm{ag}})$ in any linear flow expressed with $(\boldsymbol{U}^{\infty}, \boldsymbol{\Omega}^{\infty}, \mathsf{E}^{\infty})$, the total force, torque, and stresslet acting on it can be determined by the resistance matrix R_{ag}.

Now our problem is to find the motion of an aggregate in a shear flow. For a freely suspended aggregate, the force and torque acting on it should be zero in the small-inertia limit:

$$\boldsymbol{F}_{\mathrm{ag}} = \boldsymbol{0}, \quad \boldsymbol{T}_{\mathrm{ag}} = \boldsymbol{0}. \tag{8}$$

In order to determine $\boldsymbol{U}_{\mathrm{ag}}$ and $\boldsymbol{\Omega}_{\mathrm{ag}}$, one needs to have the inverse relation:

$$\begin{pmatrix} \boldsymbol{U}_{\mathrm{ag}} - \boldsymbol{U}^{\infty}(\boldsymbol{r}_0) \\ \boldsymbol{\Omega}_{\mathrm{ag}} - \boldsymbol{\Omega}^{\infty} \\ -\boldsymbol{E}^{\infty} \end{pmatrix} = -\mathsf{M}_{\mathrm{ag}} \cdot \begin{pmatrix} \boldsymbol{F}_{\mathrm{ag}} \\ \boldsymbol{T}_{\mathrm{ag}} \\ \boldsymbol{S}_{\mathrm{ag}} \end{pmatrix}. \tag{9}$$

The mobility matrix is the inverse matrix of the resistance matrix, $\mathsf{M}_{\mathrm{ag}} = \mathsf{R}_{\mathrm{ag}}^{-1}$. The submatrices are denoted as follows:

$$\mathsf{M}_{\mathrm{ag}} \equiv \begin{pmatrix} (\mathsf{M}_{\mathrm{ag}})_{\mathrm{UF}} & (\mathsf{M}_{\mathrm{ag}})_{\mathrm{UT}} & (\mathsf{M}_{\mathrm{ag}})_{\mathrm{US}} \\ (\mathsf{M}_{\mathrm{ag}})_{\mathrm{OF}} & (\mathsf{M}_{\mathrm{ag}})_{\mathrm{OT}} & (\mathsf{M}_{\mathrm{ag}})_{\mathrm{OS}} \\ (\mathsf{M}_{\mathrm{ag}})_{\mathrm{EF}} & (\mathsf{M}_{\mathrm{ag}})_{\mathrm{ET}} & (\mathsf{M}_{\mathrm{ag}})_{\mathrm{ES}} \end{pmatrix}. \tag{10}$$

By substituting the balancing condition (8) in Eq. (9), the stresslet acting on the aggregate is obtained as

$$\boldsymbol{S}_{\mathrm{ag}} = (\mathsf{M}_{\mathrm{ag}})_{\mathrm{ES}}^{-1} \cdot \boldsymbol{E}^{\infty}. \tag{11}$$

The strength of the stresslet S_{ag} is given as the square root of the second invariant of the tensor:

$$S_{\mathrm{ag}} \equiv \sqrt{\frac{1}{2}\sum_{j,k} (\mathsf{S}_{\mathrm{ag}})_{jk}^2}. \tag{12}$$

We refer to this quantity as the stress acting on an aggregate. At the same time, the motion of a freely suspended aggregate is determined:

$$\begin{aligned} \boldsymbol{U}_{\mathrm{ag}} &= \boldsymbol{U}^{\infty}(\boldsymbol{r}_0) - (\mathsf{M}_{\mathrm{ag}})_{\mathrm{US}} \boldsymbol{S}_{\mathrm{ag}}, \\ \boldsymbol{\Omega}_{\mathrm{ag}} &= \boldsymbol{\Omega}^{\infty} - (\mathsf{M}_{\mathrm{ag}})_{\mathrm{OS}} \boldsymbol{S}_{\mathrm{ag}}. \end{aligned} \tag{13}$$

In this way, we determine the motion under a shear flow, which in this paper is referred to as the *torque-balanced motion*.

D. Forces and moments acting on the contact points

A method to determine forces and moments acting on each contact point within an aggregate is presented in this section. Such values can be compared with the cohesive forces between colloidal particles observed in experiments. Our method is restricted to open-structured fractals, and so the application is limited. This restriction is the same as in recent work by Gastaldi and Vanni [50]. For compact aggregates, a different

approach was proposed by Bäbler *et al*. [51]. As mentioned in Sec. II A, fractal aggregates are prepared by using numerical algorithms. One common feature of such artificially generated aggregates is that the number of contact points is always $N-1$, as an addition of a particle or cluster always creates only one contact point but never creates more than two contact points at one time. This means that no loop structure can be formed in the aggregate, so that one can always divide it into two parts by cutting at an arbitrary contact point. Here we consider a contact point α at the position $\boldsymbol{r}_\alpha$, which is the unique junction to connect the two parts divided by it, named A and B. The total forces acting on each part are given by the simple summations

$$\boldsymbol{F}_{\rm A}=\sum_{i\in{\rm A}}\boldsymbol{F}^{(i)},\quad \boldsymbol{F}_{\rm B}=\sum_{i\in{\rm B}}\boldsymbol{F}^{(i)}. \tag{14}$$

For torque-balanced motion, the sum of them is zero: $\boldsymbol{F}_{\rm A}+\boldsymbol{F}_{\rm B}=\boldsymbol{0}$. These forces are supported by the cohesion at the contact point α, so the magnitude of the forces acting on α is equivalent to the total forces acting on the divided parts. The normal and sliding parts are obtained as follows:

$$F^{(\alpha)}_{\rm normal}=\boldsymbol{F}_{\rm A}\cdot\boldsymbol{n}, \tag{15}$$

$$F^{(\alpha)}_{\rm sliding}=|\boldsymbol{F}_{\rm A}-(\boldsymbol{F}_{\rm A}\cdot\boldsymbol{n})\boldsymbol{n}|, \tag{16}$$

where $\boldsymbol{n}$ is the normal vector between the adjoining particles at the contact point α. In the same way, the total moments acting on the contact point α are given as

$$\boldsymbol{M}_{\rm A}=\sum_{i\in{\rm A}}\{(\boldsymbol{r}^{(i)}-\boldsymbol{r}_\alpha)\times\boldsymbol{F}^{(i)}+\boldsymbol{T}^{(i)}\}, \tag{17}$$

$$\boldsymbol{M}_{\rm B}=\sum_{i\in{\rm B}}\{(\boldsymbol{r}^{(i)}-\boldsymbol{r}_\alpha)\times\boldsymbol{F}^{(i)}+\boldsymbol{T}^{(i)}\}. \tag{18}$$

By the same argument as above, the bending and torsional parts are obtained as

$$M^{(\alpha)}_{\rm bending}=|\boldsymbol{M}_{\rm A}-(\boldsymbol{M}_{\rm A}\cdot\boldsymbol{n})\boldsymbol{n}|, \tag{19}$$

$$M^{(\alpha)}_{\rm torsion}=|\boldsymbol{M}_{\rm A}\cdot\boldsymbol{n}|. \tag{20}$$

Thus, the forces and moments acting on all contact points ($\alpha=1,\ldots,N-1$) within a fractal aggregate can be determined.

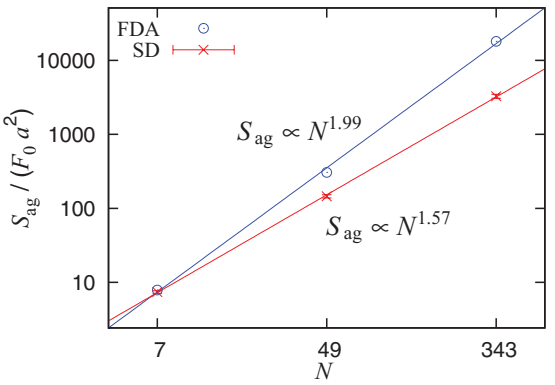

FIG. 4. (Color online) The stress $S_{\rm ag}$ normalized by F_0a^2 as obtained by the FDA and SD methods for 3D-Vicsek fractals.

III. RESULTS AND DISCUSSION

A. The torque-balanced motion of 3D-Vicsek fractals

Figure 3 shows the drag forces for three orientations of a 3D-Vicsek fractal ($N=49$) by using SD. These drag forces look similar to the flow pattern of the elongational flow given by the rate-of-strain part E^∞ of a simple shear flow. This can be understood as follows: the vortex part Ω^∞ of the simple shear flow is canceled out by the rotation of the torque-balanced motion, and the rate-of-strain part E^∞ remains to act on the aggregate.

3D-Vicsek fractals have symmetric structures. This feature is different from the two other random fractals. Because of the symmetry, the total drag force acting on the aggregate is always zero whether the FDA or SD is used, if the center of mass of the aggregate is taken as the origin of the frame of reference. Furthermore, the angular velocity at the torque-balanced motion is also always the same: $\boldsymbol{\Omega}_{\rm ag}=(G/2)\boldsymbol{e}_y$. This expected behavior was confirmed for three sizes of aggregates ($N=7,49,343$) with ten randomly chosen different orientations. Thus, the behavior of 3D-Vicsek fractals cannot be distinguished from a single sphere in a shear flow whether the FDA or SD is used.

The difference between the FDA and SD is seen by the stress $S_{\rm ag}$. When the FDA is used, it does not depend on the orientation of the aggregate, and the N dependence follows a power law $S_{\rm ag}\propto N^\lambda$ with the exponent $\lambda\approx1.99$. On the other hand, when SD is used, the stress $S_{\rm ag}$ depends slightly

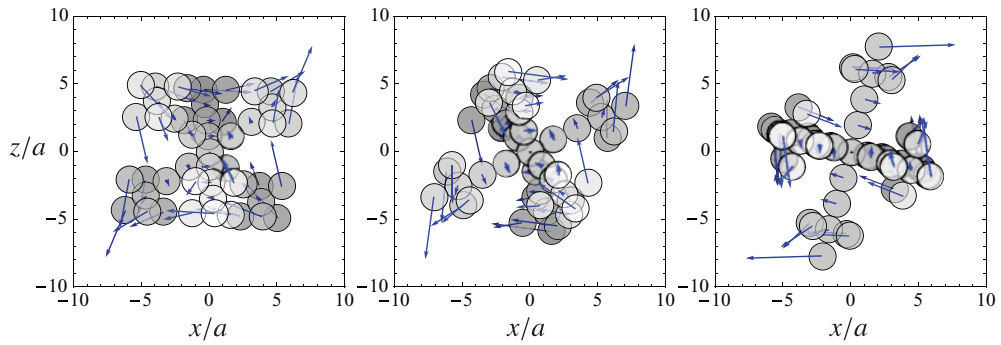

FIG. 3. (Color online) The torque-balanced motions of a 3D-Vicsek fractal ($N=49$) with three random orientations. The vectors denote the force acting on a particle, with a vector of length 2 corresponding to a force of $F_0\equiv6\pi\mu a^2G$.

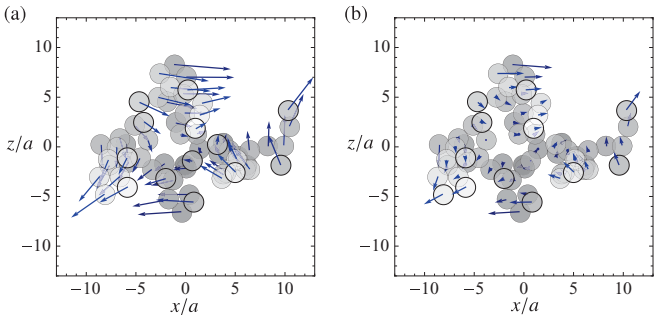

FIG. 5. (Color online) The drag forces acting on the primary particles within a CCA cluster ($N = 64$) at the torque-balanced motion. The two different methods, (a) the FDA and (b) SD, are compared. The figures show the projections for the 3D positions of the particles in the xz plane. The grayness of the circles indicate the depth of y, where darker means larger y (more behind). The drag forces are represented by the length of the vectors, where the unit of force ($F_0 \equiv 6\pi\mu a^2 G$) is set to length 1.

on the orientation of the aggregate. By using the method of least squares, the average exponent and its standard deviation are found as $\lambda \approx 1.57$. These results are shown in Fig. 4. Thus, we can see that the overestimation of stress by using the FDA increases with N. This N dependence of the stress $S_{\rm ag}$ will be further discussed in Sec. III C.

B. The torque-balanced motion of CCA clusters

Before considering the averaged behavior of CCA clusters, an individual case is discussed. A CCA cluster of 64 particles is taken here (see Fig. 5). When using the FDA, the translational velocity of the aggregate at the torque-balanced motion is zero ($\boldsymbol{U}_{\rm ag} = \boldsymbol{0}$), and the angular velocity is obtained as $\boldsymbol{\Omega}_{\rm ag}/G \approx (-0.05, 0.32, -0.02)$. With using SD, the translational velocity is obtained as $\boldsymbol{U}_{\rm ag}/aG \approx (0.21, -0.12, 0.26)$, and the angular velocity is obtained as $\boldsymbol{\Omega}_{\rm ag}/G \approx (-0.04, 0.34, 0.00)$. In any case, the torque-balanced motion is different from the case of a sphere. It rather relates to its irregular structure. In Fig. 5, the drag forces with the FDA and SD are compared. By this individual case, we can see that the magnitudes of the SD forces are much smaller than the corresponding magnitudes of the FDA.

The torque-balanced motion obviously depends on the individual structure of the samples. For open-structured aggregates, such as CCA clusters, the effect of individual structures seems significant for each torque-balanced motion. In order to see the systematic part of the results, one needs to take averages over the results of many samples. Here 256 samples of CCA clusters were calculated for each size $N = 2^{k+2}$ ($k = 1, \ldots, 8$). For the FDA the translational velocity is always zero as expected ($\boldsymbol{U}_{\rm ag} = \boldsymbol{0}$). On the other hand, for the results by SD, though the average of the velocity vectors is close to zero, the average of the magnitudes increases with the size of the aggregate. More precisely, as seen in Fig. 6(a), it is proportional to the radius of gyration, R_g, i.e., the average of the ratio between $|\boldsymbol{U}_{\rm ag}|$ and R_g remains roughly constant for different N: $\langle |\boldsymbol{U}_{\rm ag}|/R_g G \rangle \approx 0.038$. For the angular velocities $\boldsymbol{\Omega}_{\rm ag}$, the average also coincides with the case of a sphere regardless of whether the FDA or SD is used. The results for $N = 256$ are obtained as $\boldsymbol{\Omega}_{\rm ag}/G = (0 \pm 0.10, 0.50 \pm 0.18, 0 \pm 0.08)$ with the FDA and $\boldsymbol{\Omega}_{\rm ag}/G = (0 \pm 0.09, 0.50 \pm 0.16, 0 \pm 0.08)$ with SD. The standard deviation does not change appreciably with N whether the FDA or SD is used [see Fig. 6(b)]. It is remarkable that even though the aggregate becomes larger, the influence of randomness of the structure on the motion stays the same. In other words, an individual CCA cluster does not get closer to the behavior of a single sphere, even if it becomes large. However, as we will see in Sec. III C, the simplification of replacing the aggregate with a single sphere describes the situation well from a statistical viewpoint.

The stress $S_{\rm ag}$ also follows a power-law relation, $S_{\rm ag} \propto N^{\lambda}$ [see Fig. 6(c)]. The least-squares fitting leads to the following exponents: $\lambda \approx 1.92$ with the FDA and $\lambda \approx 1.47$ with SD. Though these exponents are smaller than the results for 3D-Vicsek fractals (Sec. III A), the differences of the exponents between the FDA and SD are quite similar. This N dependence of the stress will also be discussed in Sec. III C.

C. Hydrodynamic radius

Before going to the detail analysis of the drag forces, it is worth considering the obtained power laws in terms of the hydrodynamic radius. For the torque-balanced motion of fractal aggregates, we found power-law relations between the stress $S_{\rm ag}$ and the number of particles, N, in Secs. III A and III B. Because rigidity of the structure is assumed, the results

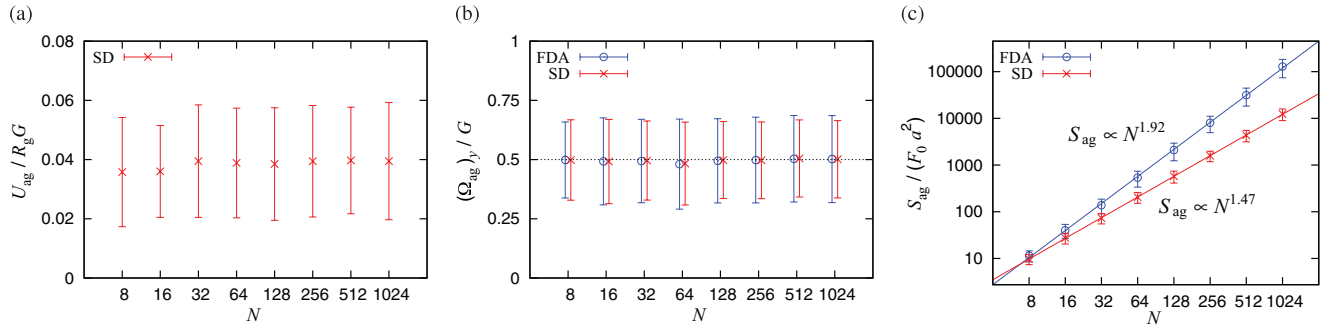

FIG. 6. (Color online) N dependence of the average translational velocity $|\boldsymbol{U}_{\rm ag}|$ (a) and the average angular velocity $(\Omega_{\rm ag})_y$ (b) of CCA clusters at the torque-balanced state. The averages are obtained over 256 samples, and the error bars indicate the standard deviations. (c) The N dependence of the stress $S_{\rm ag}$.

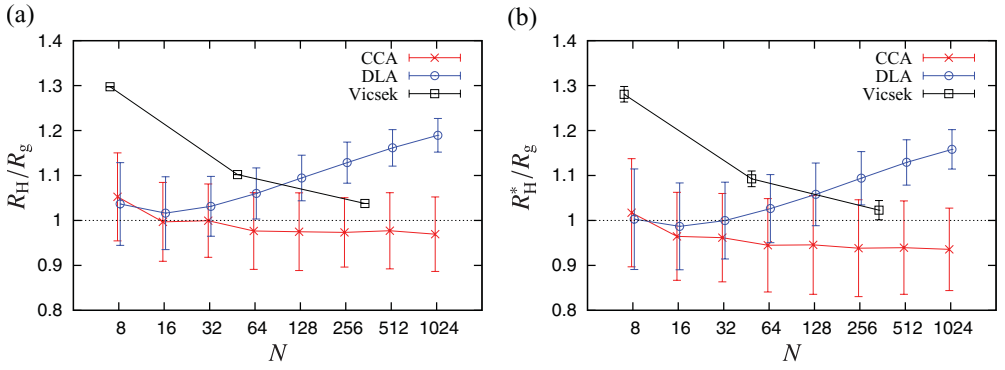

FIG. 7. (Color online) (a) The averages and standard deviations of the ratio between hydrodynamic radius and radius of gyration $\langle R_H/R_g \rangle$. (b) The averages and standard deviations of the ratio between the hydrodynamic radius in shear flow and radius of gyration $\langle R_H^*/R_g \rangle$. They were obtained over 256 samples for each size of CCA and DLA clusters and 10 samples for each size of 3D-Vicsek fractals.

obtained make sense for small aggregates. However, one can see whether or not the results obtained are reasonable by extending the power-law relation to large values of N.

First, let us consider the hydrodynamic radius R_H. The hydrodynamic radius of an aggregate is given as the corresponding radius of a sphere that gives the same drag force acting on the aggregate in a uniform flow:

$$R_H \equiv \frac{\boldsymbol{F}_{\rm ag} \cdot \boldsymbol{U}}{6\pi\mu \boldsymbol{U}^2}. \tag{21}$$

For a fractal aggregate, the radius of gyration, R_g, represents a characteristic length of the aggregate (see Sec. II A). Figure 7(a) shows the average values and standard deviations of the ratio R_H/R_g for the three types of fractal aggregates. For CCA clusters, the average ratio is about 1 and does not change with N. This result seems reasonable because the scaling behavior can be extended to larger N. In addition, similar results were reported in the literature [12,28,34,52,53]. On the other hand, the average ratio for DLA clusters slowly increases with N. If this trend is extended to larger N, the hydrodynamic effect diverges. Since such a divergence is physically unreasonable, it may represent a slow crossover to the asymptotic regime. The ratio for 3D-Vicsek fractals decreases with N and approaches 1. Though the scaling behavior is imperfect for the small aggregates, this result is physically reasonable, and similar behavior for aggregates with a lower fractal dimension was also reported by Filippov [34].

The concept of hydrodynamic radius is useful for understanding the stress in shear flow. The radius of a corresponding sphere can also be considered for the fractal aggregate in terms of stress acting on an aggregate. When a sphere with radius R is freely suspended in a shear flow, the force and torque acting on the sphere are zero, but the stress is given as

$$S_{\rm sph} = \frac{10}{3}\pi\mu R^3 G. \tag{22}$$

By using this relation, the corresponding hydrodynamic radius R_H^* is determined from the stress $S_{\rm ag}$:

$$R_H^* \equiv \left(\frac{3S_{\rm ag}}{10\pi\mu G}\right)^{1/3}. \tag{23}$$

Figure 7(b) shows the average values and standard deviations of the ratio between the hydrodynamic radius and the radius of gyration, R_H^*/R_g, for three types of fractal aggregates. Despite the different definitions of the hydrodynamic radius, we cannot see significant difference between them. This result implies that one can make use of the hydrodynamic radius estimated by sedimentation experiments to evaluate the viscosity of suspensions [14,54]. Now, the power laws obtained in Secs. III A and III B can be interpreted as the simple expectation, $S_{\rm ag} \propto R_g^3 \propto N^{3/d_f}$. Especially for CCA clusters, the hydrodynamic radius is proportional to the radius of gyration, so that the estimated exponent $3/d_f \approx 1.51$ is close to the obtained exponent 1.47. Thus, the hydrodynamic radius represents the hydrodynamic response of CCA clusters at the torque-balanced motion.

D. Drag force acting on individual particles

We saw that the stress acting on an aggregate follows a simple estimation. However, it is not obvious why such open-structured fractal aggregates show such a simple hydrodynamic response. To elucidate this behavior, the hydrodynamic interaction is investigated in greater detail. The drag forces acting on individual particles have already been shown in Fig. 5. In order to visualize the general tendency of such drag forces, the averages of the magnitudes are taken at the positions of particles. The local averages are taken by distinguishing

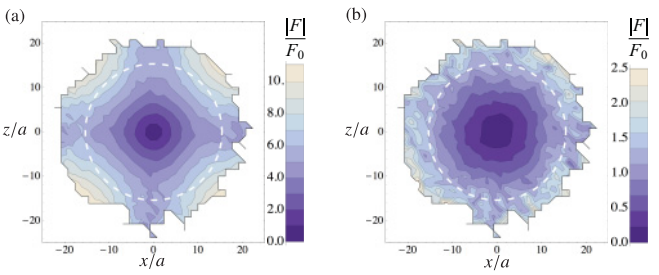

FIG. 8. (Color online) The spatial distribution of the drag force strength with (a) the FDA and (b) SD in the xz plane. The particles within the central slice $|y| < 0.1\langle R_g \rangle$ are considered. Data were averaged over 1024 CCA clusters, and the contour plots are interpolated. The plot ranges of (a) and (b) are not the same, because drag forces given by the FDA are much larger than those given by SD.

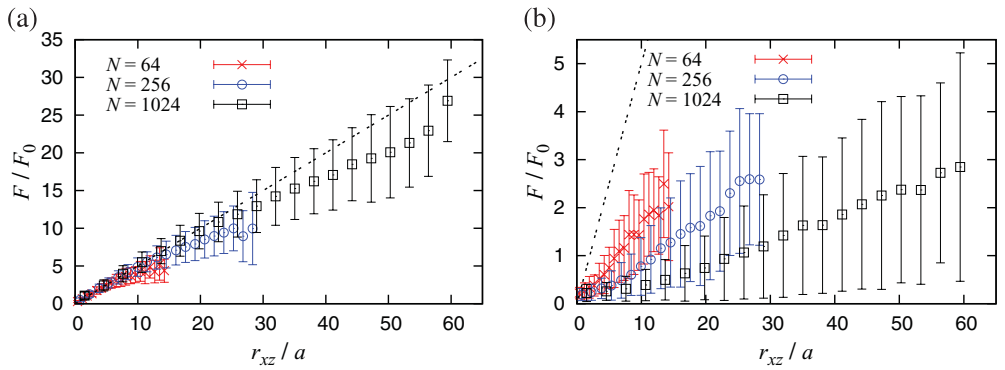

FIG. 9. (Color online) The radial dependence of drag-force strengths for CCA clusters plotted with two hydrodynamic methods, (a) the FDA and (b) SD. The error bars indicate the standard deviation. The broken line indicates the drag force $F = 3\pi\mu a G r_{xz}$, which acts on a particle that translates along the circular orbit of radius r_{xz} with velocity $\boldsymbol{v} = G/2(z, -x)$.

the positions (x,z) into square cells, $\Delta x = \Delta z = 0.1\langle R_g\rangle$. Figure 8 shows the spatial distributions in the xz plane for particles within a sliced domain $|y| < 0.1\langle R_g\rangle$, where the CCA cluster with $N = 256$ was chosen, and 1024 independent samples were calculated. There, the cells including fewer than ten data are considered as empty. The circle (with a dashed line) on the figures indicates the average radius of gyration, $\langle R_g\rangle$.

First, the remarkable reduction of the drag forces from the FDA to SD can be seen in Fig. 8. Drag forces are reduced not only inside but also throughout the entire aggregate. Second, both plots of Fig. 8 show different types of symmetric patterns. The pattern of the FDA looks to have four-fold symmetry, and the pattern of SD looks almost isotropic. The four-fold symmetry of the FDA implies a correlation between the anisotropic shape of the aggregate and the torque-balanced motion. Actually, an individual CCA cluster can have a rather different configuration from a spherical one. In shear flow, the orientation of an aggregate affects the motion and eventually the drag forces. However, we cannot present an explanation for the concentric pattern seen in the distribution of SD.

From the symmetric patterns seen in Fig. 8, we can obtain the radial dependence of the drag force. For the same sliced domain $|y| < 0.1\langle R_g\rangle$, the drag forces are averaged by the radial sections $R_j \leqslant r_{xz} < R_{j+1}$ with $j = 1, \ldots, 20$, where $R_{j+1} - R_j = 0.1\langle R_g\rangle$ and $R_1 = 0$. The results for the CCA clusters with three different sizes ($N = 16, 64, 256$) are compared in Fig. 9 for the two methods, the FDA and SD. The averages and standard deviations were obtained over 256 samples. Sections including fewer than ten data are considered as empty. It is seen that the dependence on N are significantly different between the FDA and SD. For the FDA, the slopes for the different sizes of aggregate are similar to each other, especially for smaller r_{xz}. On the other hand, for SD, the slope becomes smaller as the aggregate size increases. In these averages, the disturbance of imposed flow by particles looks systematic. However, the standard deviations of drag forces remain large even for the larger N.

We have confirmed that these systematic disturbances are more clearly seen with the radial distance normalized by the radius of gyration, r_{xz}/R_g. Figure 10 shows the six different sizes $N = 2^{k+2}$ $(k = 1, \ldots, 8)$ of CCA and DLA clusters. The drag forces $|\boldsymbol{F}^{(i)}(r_{xz})|$ are averaged over the sections by the normalized radius: $\tilde{R}_j \leqslant r_{xz}/R_g < \tilde{R}_{j+1}$ with $j = 1, \ldots, 20$, where $\tilde{R}_{j+1} - \tilde{R}_j = 0.1$ and $\tilde{R}_1 = 0$. The data closely fit on a master curve, especially for CCA clusters. This means that the average drag force depends only on the relative location within the aggregate. With the FDA, the drag force becomes larger with increasing size, because the velocity difference is simply proportional to the size of the aggregate. However, with SD the aggregate disturbs the imposed flow more and more as its size increases. As a result, the average drag force acting on one particle remains the same. The hydrodynamic interaction affecting fractal

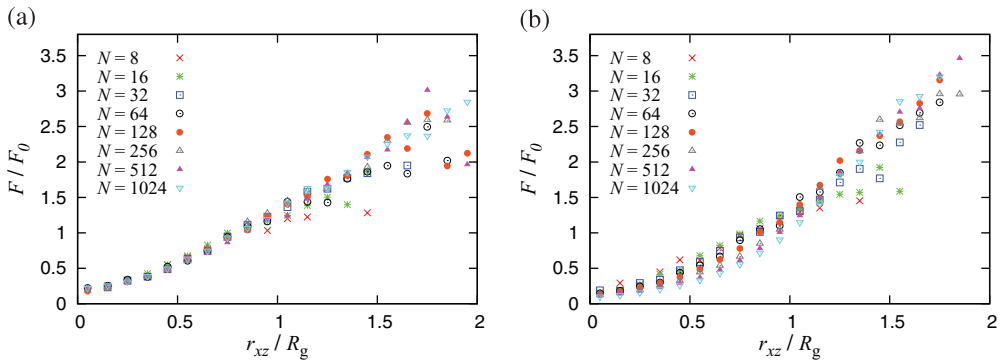

FIG. 10. (Color online) The average magnitudes of the drag forces plotted by the normalized radial distance r_{xz}/R_g, where six different sizes ($N = 8, 16, 32, 64, 128, 256$) of (a) CCA and (b) DLA clusters are plotted together, respectively.

TABLE I. The parameters used in Sec. III E to evaluate the forces and moments acting on the contact points within an aggregate.

	Symbol	Value
Viscosity of fluid	μ	0.001 Pa s
Radius of particles	a	735 nm
Shear rate	G	50 s^{-1}

aggregates can be rescaled by the radius of gyration, R_g. The same results with uniform flows were reported by Gastaldi and Vanni [50].

E. Forces and moments acting on the contact points

In order to have a concrete interpretation for the results, we consider a problem to estimate the critical size of an aggregate in shear flow. Though colloidal aggregates are known to show elastic behavior (as shown by theory [55] and direct observation [5]), we assumed that the elasticity is less effective for the small aggregates considered in this work. The interparticle bonds are considered as brittle here. When hydrodynamic stress is small, the structure of the aggregate is unchanged. As seen in Sec. III A or III B, the hydrodynamic stress becomes larger as the size of aggregate increases. When the stress at a contact point within the aggregate exceeds the cohesive force between particles, restructuring or breakup of the aggregate sets in. This critical size is discussed in this section.

The Stokes equation is a linear differential equation in terms of the velocity field and the pressure field. As a result, all derived results can be rescaled by the radius of the primary particle, a, the viscosity of the fluid, μ, and the shear rate G. In other words, there is no essential variation due to such parameters as long as the Stokes regime is valid. In this section, a set of parameters is chosen in order to demonstrate the results for some experimentally investigated system. However, the results can be translated to other systems in a straightforward way. The values of the parameters used in this examination are given by Table I. We report the maximum forces and moments acting on contact point within aggregates. These quantities also follow power-law relations with respect to the number of particles, N. Figure 11 shows the respective types of forces and moments with SD. The averages and the standard deviations are obtained over 256 samples for CCA clusters.

TABLE II. The exponents of power law seen between the maximum force/moment and number of particles: $F_{\max} \propto N^{\lambda}$ and $M_{\max} \propto N^{\lambda}$. The fitting is done with averages over 256 samples.

	CCA ($d_f \approx 1.99$)		DLA ($d_f \approx 2.31$)	
	FDA	SD	FDA	SD
Elongation	1.59	1.07	1.46	0.99
Compression	1.59	1.07	1.46	0.99
Sliding	1.54	1.03	1.45	0.99
Bending	2.06	1.56	1.84	1.40
Torsion	2.12	1.61	1.90	1.47

The exponents of the power-law relation are obtained by the method of least squares and are shown in Table II. These exponents indicate how such forces increase with the number of particles, N.

These results can be compared with the direct observation for the cohesive forces between colloidal particles reported by Pantina and Furst [4,5]. Though they observed variation by changing the chemical condition of the solvent, some typical values are taken to compare with our results, i.e., the critical elongation force and bending moment are $F_{\mathrm{Nc}} \approx 10$ pN and $M_{\mathrm{Bc}} \approx 30$ pN μm, respectively. Unfortunately, the other values are not measured in their experiments, so only the above two values are considered here. If the bonds within CCA clusters have such critical forces, the rigid regime is expected to terminate at $N \approx 63$ under a shear flow of $G = 50$ s^{-1}. There, the bending moment reaches the critical value, but the elongation force does not become critical.

For deeper understanding, we try to interpret the exponents shown in Table II. When the FDA is used, the typical forces acting on a contact point are expected to be proportional to the average drag force and to the number of particles. The average drag force is proportional to the maximum velocity difference of the imposed flow within the aggregate, which in turn is proportional to the size of aggregate. This is why one can expect the following relation: $F \propto N\Delta U \propto NR_g$. By using the fractal relation (1), the exponent of such a force is estimated as

$$\lambda_{\mathrm{force}}^{(\mathrm{FDA})} \approx 1 + \frac{1}{d_f}. \tag{24}$$

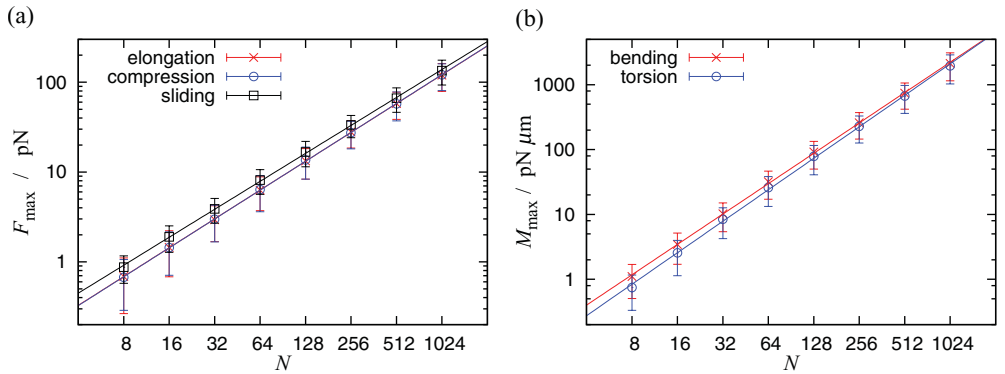

FIG. 11. (Color online) The averages of the (a) maximum forces and (b) moments acting on the contact points within aggregates obtained over 256 CCA clusters. The drag forces were calculated by using SD.

This is 1.50 and 1.43 for CCA and DLA clusters, respectively, which are roughly comparable to the obtained exponents for the maximum elongation force, i.e., 1.59 and 1.46. For the results of SD, we saw in Sec. III D that the drag-force distributions do not depend on the size of an aggregate, if the position is rescaled by R_g. This implies that the typical force acting on a contact point is expected to increase only with the number of particles: $F \propto N$; that is, the exponent is 1. Actually, the obtained exponents for the maximum elongation force are 1.07 and 0.99 for CCA and DLA clusters, respectively. The typical moments acting on a contact point are expected to be the product of force and the typical length of the aggregate: $M \propto F R_g$, which leads to the following relation between the exponents:

$$\lambda_{\mathrm{moment}}^{(\mathrm{FDA})} \approx 1 + \frac{2}{d_f}, \quad \lambda_{\mathrm{moment}}^{(\mathrm{SD})} \approx 1 + \frac{1}{d_f}. \tag{25}$$

From this the $\lambda_{\mathrm{moment}}^{(\mathrm{FDA})}$ should be 2.01 and 1.87 for CCA and DLA clusters, respectively, which are roughly comparable to the obtained exponents for the maximum bending moment, i.e., 2.06 and 1.84. $\lambda_{\mathrm{moment}}^{(\mathrm{SD})}$ values are 1.50 and 1.43, respectively, which are roughly comparable to the obtained exponents for the maximum bending moment, i.e., 1.56 and 1.40. Thus, the simple estimations roughly explain the N dependence of the maximum forces and moments acting on the contact points.

IV. SUMMARY AND CONCLUSION

We have evaluated the hydrodynamic interaction acting on rigid fractal aggregates using Stokesian dynamics. Freely suspended aggregates follow the imposed shear flow, and the torque-balanced motion is introduced in order to investigate such a situation statistically. We have found that the hydrodynamic radius of the fractal aggregates scales proportionally with their radius of gyration, R_g. Even for small aggregates, the average drag-force distribution fits on a master curve if one uses a normalized radial distance r/R_{ag}. It has also been confirmed that the stress-radius relation $S_{\mathrm{ag}} \propto R_g^3$ is valid even for small CCA clusters. As a demonstration, we have calculated that the critical size at which the aggregate no longer remains rigid is of a few tens of particles if we take the typical cohesive force for colloidal particles.

In this work, we have assumed a rigid structure for the fractal aggregates. However, the effect of elasticity is expected to increase for larger aggregates [55]. If such elasticity is taken into account, the size dependence of the mechanical stability threshold could be weaker than that estimated in this work. In addition, no restructuring has been dealt with in this work. If loops are formed because of restructuring, the aggregates becomes more and more robust. In order to know the final size and morphology of colloidal aggregates in shear flow, such an effect needs to be studied.

ACKNOWLEDGMENTS

The authors would like to thank Dr. K. Ichiki for providing the simulator of Stokesian dynamics RYUON and for much instructive advice, Ms. E. C. Schlauch and Mr. M. Ernst for useful discussions, and Dr. A. M. Reilly for assistance with the manuscript. We also acknowledge the financial support of the German Science Foundation (DFG priority program SPP 1273).

[1] W. A. Ducker, T. J. Senden, and R. M. Pashley, Nature (London) **353**, 239 (1991).
[2] L.-O. Heim, J. Blum, M. Preuss, and H.-J. Butt, Phys. Rev. Lett. **83**, 3328 (1999).
[3] S. Ecke, R. Raiteri, E. Bonaccurso, C. Reiner, H.-J. Deiseroth, and H.-J. Butt, Rev. Sci. Instrum. **72**, 4164 (2001).
[4] J. P. Pantina and E. M. Furst, Langmuir **20**, 3940 (2004).
[5] J. P. Pantina and E. M. Furst, Phys. Rev. Lett. **94**, 138301 (2005).
[6] A. D. Dinsmore and D. A. Weitz, J. Phys. Condens. Matter **14**, 7581 (2002).
[7] D. W. Schaefer, J. E. Martin, P. Wiltzius, and D. S. Cannell, Phys. Rev. Lett. **52**, 2371 (1984).
[8] K. Wong, B. Cabane, R. Duplessix, and P. Somasundaran, Langmuir **5**, 1346 (1989).
[9] S. Stone, G. Bushell, R. Amal, Z. Ma, H. G. Merkus, and B. Scarlett, Meas. Sci. Technol. **13**, 357 (2002).
[10] A. S. Michaels and J. C. Bolger, Ind. Eng. Chem. Fundam. **1**, 24 (1962).
[11] P. M. Adler, AIChE J. **25**, 487 (1979).
[12] P. Wiltzius, Phys. Rev. Lett. **58**, 710 (1987).
[13] G. Pranami, M. H. Lamm, and R. D. Vigil, Phys. Rev. E **82**, 051402 (2010).
[14] R. Wessel and R. C. Ball, Phys. Rev. A **46**, 3008 (1992).
[15] R. C. Sonntag and W. B. Russel, J. Colloid Interface Sci. **113**, 399 (1986).
[16] T. Serra and X. Casamitjana, J. Colloid Interface Sci. **206**, 505 (1998).
[17] C. Selomulya, R. Amal, G. Bushell, and T. D. Waite, J. Colloid Interface Sci. **236**, 67 (2001).
[18] C. Selomulya, G. Bushell, R. Amal, and T. D. Waite, Int. J. Miner. Process. **73**, 295 (2004).
[19] V. A. Tolpekin, M. H. G. Duits, D. van den Ende, and J. Mellema, Langmuir **20**, 2614 (2004).
[20] M. Soos, J. Sefcik, and M. Morbidelli, Chem. Eng. Sci. **61**, 2349 (2006).
[21] M. Soos, A. S. Moussa, L. Ehrl, J. Sefcik, H. Wu, and M. Morbidelli, J. Colloid Interface Sci. **319**, 577 (2008).
[22] L. Ehrl, M. Soos, and M. Morbidelli, Langmuir **24**, 3070 (2008).
[23] A. Zaccone, M. Soos, M. Lattuada, H. Wu, M. U. Bäbler, and M. Morbidelli, Phys. Rev. E **79**, 061401 (2009).
[24] Y. M. Harshe, M. Lattuada, and M. Soos, Langmuir **27**, 5739 (2011).
[25] D. F. Bagster and D. Tomi, Chem. Eng. Sci. **29**, 1773 (1974).
[26] P. M. Adler and P. M. Mills, J. Rheol **23**, 25 (1979).
[27] R. C. Sonntag and W. B. Russel, J. Colloid Interface Sci. **115**, 378 (1986).
[28] W. V. Saarloos, Physica A **147**, 280 (1987).
[29] S. Kim and S. J. Karrila, *Microhydrodynamics* (Dover, New York, 2005).

[30] V. Becker, E. Schlauch, M. Behr, and H. Briesen, J. Colloid Interface Sci. **339**, 362 (2009).
[31] G. Bossis, A. Meunier, and J. F. Brady, J. Chem. Phys. **94**, 5064 (1991).
[32] C. Binder, C. Feichtinger, H.-J. Schmid, N. Thürey, W. Peukert, and U. Rüde, J. Colloid Interface Sci. **301**, 155 (2006).
[33] Y. M. Harshe, L. Ehrl, and M. Lattuada, J. Colloid Interface Sci. **352**, 87 (2010).
[34] A. V. Filippov, J. Colloid Interface Sci. **229**, 184 (2000).
[35] K. Higashitani, K. Iimura, and H. Sanda, Chem. Eng. Sci. **56**, 2927 (2001).
[36] S. Harada, R. Tanaka, H. Nogami, and M. Sawada, J. Colloid Interface Sci. **301**, 123 (2006).
[37] R. Jullien and R. Botet, *Aggregation and Fractal Aggregates* (World Scientific, Singapore, 1987).
[38] P. Meakin, J. Sol-Gel Sci. Technol. **14**, 97 (1999).
[39] D. A. Weitz and M. Oliveria, Phys. Rev. Lett. **52**, 1433 (1984).
[40] R. Botet, R. Jullien, and M. Kolb, J. Phys. A: Math. Gen. **17**, 75 (1984).
[41] T. A. Witten and L. M. Sander, Phys. Rev. B **27**, 5686 (1983).
[42] M. Y. Lin, R. Klein, H. M. Lindsay, D. A. Weitz, R. C. Ball, and P. Meakin, J. Colloid Interface Sci. **137**, 263 (1990).
[43] L. Durlofsky, J. F. Brady, and G. Bossis, J. Fluid Mech. **180**, 21 (1987).
[44] J. F. Brady and G. Bossis, Annu. Rev. Fluid Mech. **20**, 111 (1988).
[45] K. Ichiki, J. Fluid Mech. **452**, 231 (2002).
[46] K. Ichiki, RYUON simulation library for Stokesian dynamics (2011).
[47] M. Doi and D. Chen, J. Chem. Phys. **90**, 5271 (1989).
[48] A. A. Potanin, J. Colloid Interface Sci. **157**, 399 (1993).
[49] V. Becker and H. Briesen, J. Colloid Interface Sci. **346**, 32 (2010).
[50] A. Gastaldi and M. Vanni, J. Colloid Interface Sci. **357**, 18 (2011).
[51] M. U. Bäbler, M. Morbidelli, and J. Baldyga, J. Fluid Mech. **612**, 261 (2008).
[52] S. N. Rogak and R. C. Flagan, J. Colloid Interface Sci. **134**, 206 (1990).
[53] M. Lattuada, H. Wu, and M. Morbidelli, J. Colloid Interface Sci. **268**, 96 (2003).
[54] G. K. Batchelor, J. Fluid Mech. **41**, 545 (1970).
[55] Y. Kantor and I. Webman, Phys. Rev. Lett. **52**, 1891 (1984).